RSC Advances

PAPER

View Article Online
View Journal | View Issue

Cite this: *RSC Adv.*, 2015, **5**, 6553

Short ligands offer long-term water stability and plasmon tunability for silver nanoparticles†

Serene Bayram, Omar K. Zahr and Amy Szuchmacher Blum*

Received 2nd September 2014
Accepted 18th December 2014

DOI: 10.1039/c4ra09667c

www.rsc.org/advances

Four short ligands; cysteine, cysteamine, dithiothrietol and glycine are examined and compared in their ability to stabilize and assemble silver nanoparticles (AgNPs). Transmission Electron Microscopy (TEM) and UV-visible spectroscopy are used to characterize these nanoparticles in terms of their size (7–16 nm), stability, and capacity for inter-particle assembly and plasmon coupling enforced by hydrogen-bonding. The results show that both sulfhydryl and amine groups can interact with the silver nanoparticle surface. The polydispersity of glycine-stabilized AgNPs can be significantly reduced by centrifugal filtration using an appropriate membrane pore size.

Introduction

There is a great deal of interest in the controlled synthesis of noble metal nanoparticles that can be largely attributed to their versatile applications in various fields including electronics,[1,2] catalysis,[3] optics,[4,5] biological labeling[6] and surface-enhanced Raman spectroscopy (SERS).[7,8] Nobel metal nanoparticles can support localized surface plasmon resonances (LSPRs) – coherent oscillations of conduction band electrons in response to specific wavelengths of light – which can result in an extraordinary enhancement of local electromagnetic fields in the junction between two adjacent metal particles.[9] These junctions or "hot spots", have a focusing effect on electromagnetic field intensity.[10] Plasmon coupling has been employed to develop molecular plasmon rulers, as an alternative to Förster Resonance Energy Transfer (FRET) rulers, due to the increased photostability and larger extinction cross sections of plasmonic metal nanoparticles in comparison to common fluorophores.[11]

AgNPs are frequently synthesized by chemical reduction of a silver salt to yield colloidal spherical silver NPs with diameters of several nanometers.[12] Unfortunately, AgNPs have a high surface energy, and consequently, poor colloidal stability. To alleviate this problem, stabilizing molecules or ligands are employed to manipulate electrostatic repulsion or steric hindrance and prevent aggregation. There are several methodologies for silver nanoparticle synthesis that provide various advantages. For example, the use of polysaccharides as stabilizing molecules or templating matrices for silver salt reduction provides a more environmentally sustainable synthetic route.[13] Tollen's reagent, diamminesilver(I) – commonly used to test for the presence of aldehydes – can also be used to generate silver nanoparticles with good size control through the reduction of silver ions with aldehydes.[14] Reductant free methods include laser irradiation followed by polymer stabilization,[15] bio-assisted reduction and stabilization,[16] and the use of polyoxometalates (POMs) that serve as reducing and stabilizing agents as well as photocatalysts.[17,18] Certain ligands can provide a mechanism for inter-particle self-assembly in addition to colloidal stabilization. Previous strategies have involved the use of hydrogen-bonding[19] and DNA[20] self-assembly. Such platforms have the dual purpose of providing colloidal stability as well as a handle for two- or three-dimensional self-assembly. Unfortunately, despite these efforts, the synthesis of aqueous-stable and monodisperse silver NPs remains a significant challenge.

In this study, we report a green and facile aqueous synthesis of silver nanoparticles by chemical reduction and their stabilization by four short molecules: glycine, cysteine, cysteamine, and dithiothreitol (DTT). To the best of our knowledge, cysteine is the only amino acid previously used to stabilize silver nanoparticles through silver–sulfide bonding to date,[19] however, these particles tend to form networks driven by hydrogen bonding under ambient conditions which prevents their effective dispersion and complicates size purification. We have also observed significant cross-linking in solutions of cysteamine and DTT-stabilized particles. For cysteine stabilized NPs, the effect is slightly subdued by mutual repulsion between carboxylate moieties. Ag–glycine NPs showed no appreciable cross-linking and a bimodal size distribution. The presence of the various ligands at the surface of the silver colloids is confirmed by FT-IR spectroscopy. Finally, we also examine the effect of increasing the ionic strength with NaCl on the aggregation of the particles and suggest that repulsive hydration is minimal. TEM and DLS analyses are consistent with the electrical double layer theory (EDL).[21]

Department of Chemistry and Centre for Self-Assembled Chemical Structures, McGill University, 801 Sherbrooke Street West, Montreal, QC, H3A 0B8, Canada. E-mail: amy.blum@mcgill.ca; Tel: +1 5143986237

† Electronic supplementary information (ESI) available. See DOI: 10.1039/c4ra09667c

Experimental section

Materials

All chemicals were used without further purification. $AgNO_3$ (>99%, Aldrich), $NaBH_4$ (98%, Aldrich), glycine (98%, Acros), cysteamine (95%, Aldrich), DL-dithiothreitol (Biotechnology grade, Fischer), and L-cysteine (97%, Aldrich). NaCl (>99%) was purchased from ACP chemicals (Montreal, QC). Deionized water (>18 MΩ) was used and obtained using Barnstead Diamond TII (Thermo Fisher) purification system. Centrifugations were performed with a SORVALL RC 6 PLUS centrifuge (Thermo Fisher Scientific, Waltham, MA) using an SH-3000 swinging rotor. Centrifugal filtration of Ag–glycine nanoparticles was carried out using a tabletop fixed angle centrifuge (SORVALL Pico Instrument).

Synthesis and purification of glycine-stabilized AgNPs

$AgNO_3$ (10.0 μmol) was dissolved in 100 mL of water (or saline solution of desired ionic strength) at room temperature and chemically reduced by an excess of cold $NaBH_4$ (0.012 g) giving the characteristic yellow color of AgNP colloid. The reduction was accompanied by the release of hydrogen gas due to hydride oxidation. Excess sodium borohydride is hydrolysed into sodium borate. 2 mL of 2 mM glycine solution was then added and the solution (pH = 9.95) was stirred for 10 minutes and left to age for 24 hours in the dark. The glycine at this pH is negatively charged as its isoelectric point is 5.97. Particles were concentrated and excess reagents were washed away by centrifuging at 3000 × *g* through regenerated cellulose membranes (MWCO 3 kDa) twice for 30 min intervals. Large aggregates were separated, narrowing the size distribution of the Ag–gly particles, by spinning the NPs across 100 kDa membrane filters at 4000 rpm for 30 min. The particles were stored at room temperature in the dark and were stable for at least three months.

Cysteine, cysteamine and DTT modified AgNPs

For the cysteine, cysteamine, and DTT-stabilized AgNPs, the same procedure was followed; however, the stability of the prepared nanoparticles was strongly dependent on the [$AgNO_3$]/[ligand]. All ligand solutions were initially bubbled with N_2 to remove oxygen and prevent thiol oxidation. After reducing 1.7 mg of $AgNO_3$ with 1.5 mg of $NaBH_4$, 250 μL of 3.3 mM cysteine solution were added to stabilize the AgNPs. The yellow color immediately changed to clear orange. For the cysteamine and DTT stabilized AgNPs, 500 μL of 3.9 mM and 300 μL of 6.5 mM of cysteamine and DTT solutions respectively were used. The pH of the prepared nanoparticles ranged between 9.5 and 10. The as-prepared cysteine and DTT stabilized AgNPs were stable at ambient conditions for months, and the cysteamine-capped AgNPs were stable for one month in the given pH. The colloids were concentrated using centrifugation through 3000 or 3500 Da regenerated cellulose membranes at 3500 rpm using a swinging bucket centrifuge or at 8500 rpm using a fixed-angle centrifuge for at least 30 min (Fig. 1).

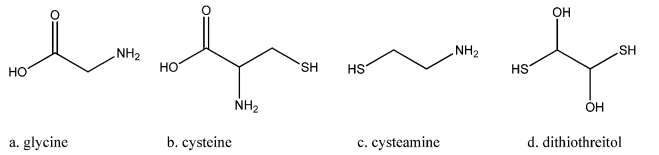

Fig. 1 The structural formulae of the four ligands: (a) glycine, (b) cysteine, (c) cysteamine in its reduced form (cysteamine oxidizes to cystamine forming a disulfide, so it was delicately handled and flushed with N_2 prior to use) and (d) DTT.

UV-vis, TEM and DLS characterisation

UV-visible extinction spectra in the 200–800 nm region were collected using a Cary 100 Bio instrument. The size, morphology and size distribution were characterized by TEM. Samples were plated on 200 mesh carbon-coated copper grids (Canemcoe-Marivac, Lakefield, QC) for 5 min before wicking using filter paper. Images were collected using a Tecnai 12 TEM at 120 kV. Analysis of TEM images was carried out using ImageJ 1.43u (Wayne Rasband, National Institutes of Health, USA). Batch mode hydrodynamic size measurements were performed using 90Plus particle size analyzer (Brookhaven). Samples were prepared as described above and filtered through a pre-rinsed 0.2 μm filter before a minimum of three measurements per sample were made.

Zeta (ζ) potential measurements

ζ potential values (mV) were obtained using a Zetaplus analyzer (Brookhaven Instruments, Holtsville, NY) supplied with a laser line of 633 nm. Each ζ potential value is reported as an average of ten measurements for each sample.

FT-IR spectroscopy

The FT-IR spectra were collected using a Spectrum Two FT-IR spectrometer supplied with an ATR diamond crystal recessed on a metal plate to ensure a good retention of the sample. A 25-fold concentrated sample of the AgNPs was dropped on the crystal and left to dry in air before measurement.

Results and discussion

Fig. 2A shows the absorption spectra of the silver nanoparticles stabilized by the four types of ligands. A shift in the plasmon band position is observed from 389 nm for Ag–gly, to 400 nm for Ag–cysteine, 430 nm for Ag–DTT and 400 nm for Ag–cysteamine. An additional peak appears at 592 nm for Ag–cysteamine, and it persists for other cysteamine concentrations. This double peak effect has been observed in cysteamine-modified gold NPs which exhibited a second band at 750 nm in addition to the characteristic 525 nm plasmon resonance band.[22] Similarly, Lin and coworkers have shown that capping 13 nm gold nanoparticles with 2-mercaptoethanol led to their assembly into branched chains, interconnected networks and loops, giving rise to a longitudinal plasmon band generated by the coupling of adjacent dipolar plasmons.[23] The low-energy band that appears in the extinction spectrum of the cysteamine-modified

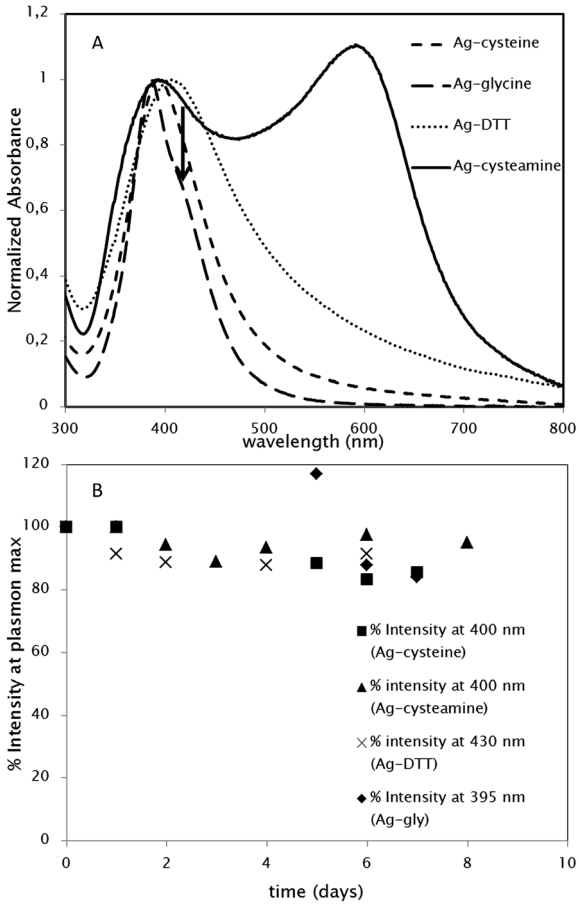

Fig. 2 (A) Absorption spectra of the silver colloids prepared with the four types of ligands: glycine, cysteine, DTT and cysteamine. The spectra were normalized to the absorbance value at λ_p of each type of ligands. (B) Change in % plasmon intensity for AgNPs capped with the four types of ligands with time.

AgNPs can be explained by an analogous plasmon coupling occurring between neighboring nanoparticles, driven by hydrogen bonding between adjacent cysteamine molecules. The largest red-shift of 39 nm is observed in the presence of DTT, likely due to the higher nucleophilicity of this ligand, and the possibility of a bidentate ligand binding to the AgNP surface.

Previously, DTT was successfully used as an efficient displacement molecule of functional ligands on gold nanoparticles surface to quantify them owing to its strong affinity to gold.[24] In addition to the large red-shift, the extinction spectrum of the DTT-stabilized AgNPs also shows the broadest plasmon band in comparison with the other three ligands. The broadness and red-shift of the plasmon band are attributed to compact aggregation of the nanoparticles driven by dipole–dipole interactions as well as hydrogen-bonding. This interpretation is consistent with an extinction coefficient simulation based on the discrete dipole approximation (DDA) of an aggregate made up of 245 gold nanoparticles, which showed broadening and red-shifting of the discrete nanoparticle plasmon from 520 nm to 570 nm,[23] analogous to what is observed here in the silver nanoparticle system.

Fig. 2B depicts the change in the % extinction intensity for AgNPs at their respective λ_p. Ag–glycine is mainly electrostatically stabilized by the carboxylate groups ($\zeta = -47.84$ mV at solution pH). A weak shoulder indicated by an arrow is due to minimal aggregation that is also noticed in TEM (Fig. 4A). Ag–cysteine has a lower ζ of -24 mV and still showed long-term water stability despite the slight plasmon broadening that is noticed over time at the expense of plasmon intensity at λ_p, which relatively decreased to 84% in one week. The consistency in plasmon peak intensity over time demonstrates the stability of the samples *vs.* aggregation.

In contrast to aggregation due to instability, the broadening of the plasmon bands and the clear emergence of a distinct longitudinal band in the presence of DTT and cysteamine respectively take place immediately upon the addition of the ligand. The plasmon bandwidths were also stable over time (Fig. SI-1†). Recording a ζ value for Ag–cysteamine and Ag–DTT was hindered due to the high absorbance of the former at 633 nm as well as the absence of charged groups on DTT in the latter. The stability of these particles, which is also dependent on ligand : AgNP ratio (Fig. SI-2B†), is possibly explained by the hydroxyl and amine H-bonding with solvent molecules.

In the case of Ag–gly, glycine binds to the Ag surface through the amine group, exposing the carboxylates to the solvent, which imparts a negative surface charge to the NPs. Fig. 3A shows the FT-IR bands corresponding to the glycine molecule: 506 cm^{-1} for CO_2 rocking, 601 cm^{-1} for CO_2 wagging, 697 cm^{-1} for CO_2 bending, 893 cm^{-1} for CC + CN stretching, 1035 cm^{-1} for CN and CC stretching, 1110 cm^{-1} for NH_3 rocking, 1328 cm^{-1} for CH_2 wagging, 1410 cm^{-1} for CO_2 symmetric stretching.[25] The persistence of the CO_2 stretching suggests that most of the carboxylates are left free, unbound to the AgNP surface. The relatively large negative zeta potential of Ag–glycine NPs at a pH of 9.8 is consistent with free carboxylates at the nanoparticle surface, which play a strong role in maintaining a good dispersion of the NPs through charge stabilization.

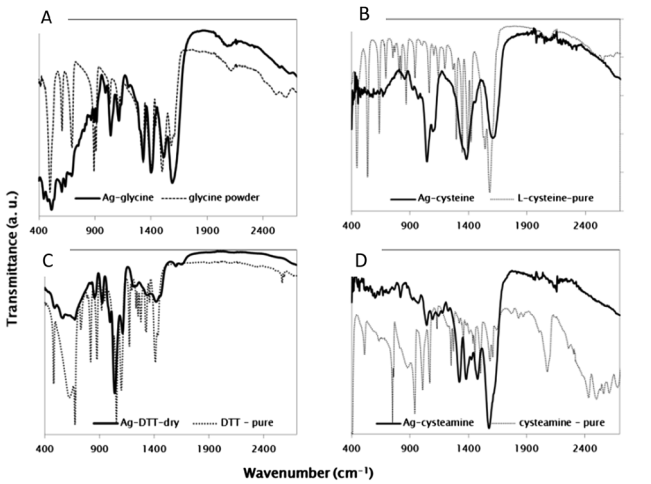

Fig. 3 FT-IR spectra of the dried concentrates of (A) Ag–glycine, (B) Ag–cysteine, (C) Ag–DTT and (D) Ag–cysteamine. Spectra of pure ligands are presented in the dotted traces.

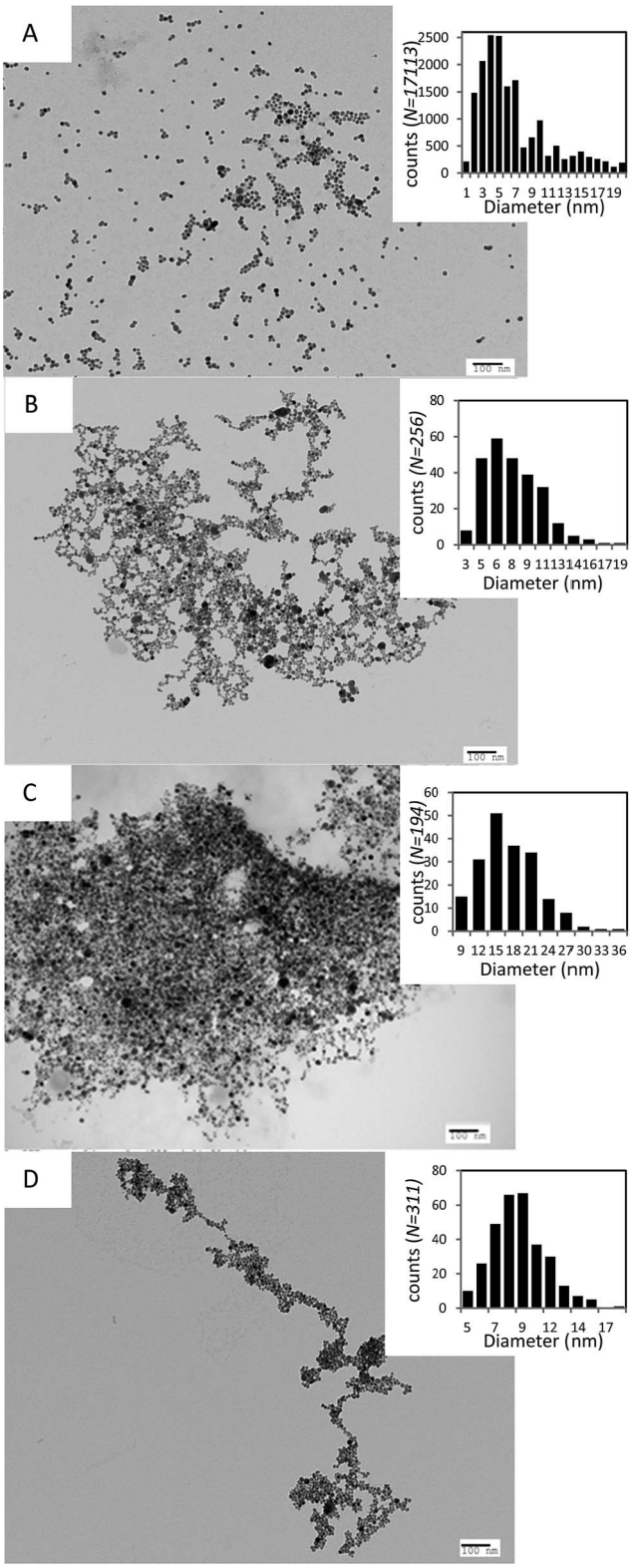

Fig. 4 TEM micrographs of (A) Ag–glycine; (B) Ag–cysteine; (C) Ag–DTT; (D) Ag–cysteamine. Insets are the size distribution histograms with the total number of NPs analysed indicated.

In the Ag–cysteine system, we observe possible cross-linking between nanoparticles as suggested by TEM images (Fig. 4B) and broadening in the plasmon band (Fig. 2A). The FT-IR data suggests that no bidentate thiol–amine coordination to the NP occurs (Fig. 3B). The disappearance of the SH stretching vibration at 2540 cm^{-1} and the SH bending at 940 cm^{-1} demonstrates that the thiol binds to the nanoparticle surface. However, although the NH_3 symmetric bending at 1347 cm^{-1} is weakened for Ag–cysteine, the NH_3 asymmetric bending at 1581–1594 cm^{-1} persists when the ligand is bound to AgNP. The observed weakening in the NH_3 bend could be due to H-bonding in the nanoparticle system. If this were due to bidentate binding to the nanoparticle surface, the asymmetric bend would also reduce in intensity, in contrast to the observed spectrum. The availability of free amines for hydrogen bonding is consistent with the cross-linking and networking of the NPs as revealed by TEM (Fig. 4B) and by Mandal *et al.*[19] Recalling that the pH of the silver nanoparticle solutions is 9.8–10, and that the pK_a of the α-amino group in cysteine is 10.25, the deprotonated form of the amines – which is capable of hydrogen bonding – is predominant. If the silver surface interacted strongly with both the sulfhydryl and the amino groups present on cysteine, the electrostatic repulsion produced by carboxylates at this pH would have produced electrostatically dispersed nanoparticles as shown for glycine stabilized nanoparticles. The measured zeta potential has a reduced value of −24.06 mV, almost half the value for glycine stabilized nanoparticles, which is consistent with the FT-IR spectrum showing that the silver surface interacts with the sulfhydryl groups alone.

For DTT-stabilized nanoparticles, both UV-visible and FT-IR spectroscopy support the bidentate binding of both thiol groups to the surface. Fig. 3C shows the FT-IR spectrum for the DTT-modified AgNPs. The CS and CC stretches appear between 635 and 730 cm^{-1}. The occurrence of bidentate binding is supported by the absence of SH bending (942 cm^{-1}) and stretching (2546 cm^{-1}) vibrational modes in the corresponding FT-IR spectrum in Fig. 3C, suggesting that most of the DTT thiols are bound to the silver surface. The FT-IR spectrum of Ag–cysteamine also indicates the preferential binding of cysteamine to AgNPs through its sulfhydryl group.

Fig. 4 shows TEM micrographs of AgNPs stabilized by the different ligands taken on the same day of the particles synthesis. The glycine stabilized nanoparticles are well-dispersed on the TEM grid, with an average size of 6.8 nm. In contrast, evidence for cross-linking is observed in the cases of cysteine, DTT and cysteamine. As Fig. 4B shows, extended nanoparticle chains are observed for Ag–cysteine nanoparticles, consistent with prior observations.[19] Ag–cysteamine shows a much more extensive nanoparticle network formation (Fig. 4D). As lower energy bands were observed for all observed cysteamine concentrations in UV-visible spectra (Fig. SI-3A†), both TEM and solution measurements are consistent with extensive hydrogen bonding in these particles, indicating a higher propensity for hydrogen bonding as compared to the other ligands. The aggregation of the NPs in the presence of cysteamine is accompanied by a respective increase and decrease of the longitudinal and axial bands, respectively, until a steady state is reached in almost one hour after which no further aggregation occurs (Fig. SI-3B†). The protonation of amines in acidic medium hinders the NPs crosslinking due to reduced

H-bonding as the N–H bonds become less polarized as depicted in Fig. 5. In the case of DTT, we observe a more compact aggregate structure, with no apparent chains or rings (Fig. 4C), as suggested by the broadening observed in the UV-visible spectrum.

Although the DTT and cysteamine-modified AgNPs show a great deal of hydrogen bonding aggregation due to their NH_2 and OH or SH moieties respectively, these ligands provide long term stability for silver nanoparticles in aqueous solution. The strength of the silver–thiol binding in the cases of cysteine, DTT, and cysteamine affords a good passivation of the surface, which minimizes undesired van der Waals driven aggregation. This stability, as well as the plasmon band properties, are greatly dependent on the [Ag] : [ligand] ratio, which can impact both the surface coverage and the degree of hydrogen bonding. This relationship is currently under systematic investigation. TEM revealed an average size of 7.8 ± 1.9 nm for the Ag–cysteine NPs, 15.8 ± 3.2 nm for the Ag–DTT NPs and 9.7 ± 2.3 nm for Ag–cysteamine NPs. The respective average hydrodynamic diameters (HDD) for Ag–cysteine and Ag–DTT NPs as determined by DLS are 44 nm and 41 nm. The Ag–cysteamine NPs strongly absorb at 633 nm, making it difficult to obtain useful HDD data. The Ag–glycine NPs had a smaller HDD of 30 nm, which is in accordance with their higher zeta potential due to the smaller size of their electrokinetic units. The comparable HDDs of Ag–cysteine and Ag–DTT suggest possible H-bonding between the ligands and the solvent molecules, which promotes good water stability. TEM micrographs of AgNPs colloids taken at later periods of time did not reveal significant change in morphology or aggregation of the particles (Fig. SI-4†). This is consistent with the UV-vis spectra presented in Fig. SI-1,† which show a slight intensity drop at λ_p within the first day of synthesis, after which a steady plasmon band persists.

Unlike the other ligands, the glycine doesn't offer a hydrogen bonding moiety that could drive other ligand molecules onto the NP surface, ending up in poor coverage of the surface. The poor coverage in turn exposes considerable surface areas which paves the way for dipole–dipole attractive van der Waals forces to cause aggregation of the NPs according to the DLVO theory,[26] suggesting that glycine stabilized nanoparticles will be highly sensitive to solution ionic strength.

The effect of increasing the ionic strength of the Ag–gly colloid with a strong electrolyte like NaCl was studied by DLS and TEM. Fig. 6 shows the amplified aggregation upon increasing the ionic strength from 5 to 15 mM. Ionic strengths higher than 15 mM resulted in colloidal destabilization and precipitation. Furthermore, increasing the salt concentration promotes rapid Ostwald ripening of the nanoparticles. The TEM measured diameter of the NPs increased from 13.5 ± 5 nm at $[I] = 5$ mM to 16.8 ± 6 nm at $[I] = 10$ mM to 28 ± 15 nm at $[I] = 15$ mM. This result is in agreement with the electrical double layer (EDL) theory that describes the diffuse layer thickness ($\bar{k}$, nm) that separates the Stern layer around the colloidal particle from the bulk of the solution, and whose value is inversely proportional to the square root of the ionic strength of the medium according to the following relation where λ_B is the Bjerrum length of the medium (0.7 nm for water at room temperature).

$$\kappa^{-1} = \frac{1}{\sqrt{8\pi\lambda_B N_A I}}$$

The reduction in the diffuse layer thickness upon increasing the ionic strength favors the interaction between the Ag–gly particles where the van der Waals forces outweigh the repulsive forces leading to aggregation. Thus, while glycine is an effective stabilizing surface ligand in water, incomplete coverage results

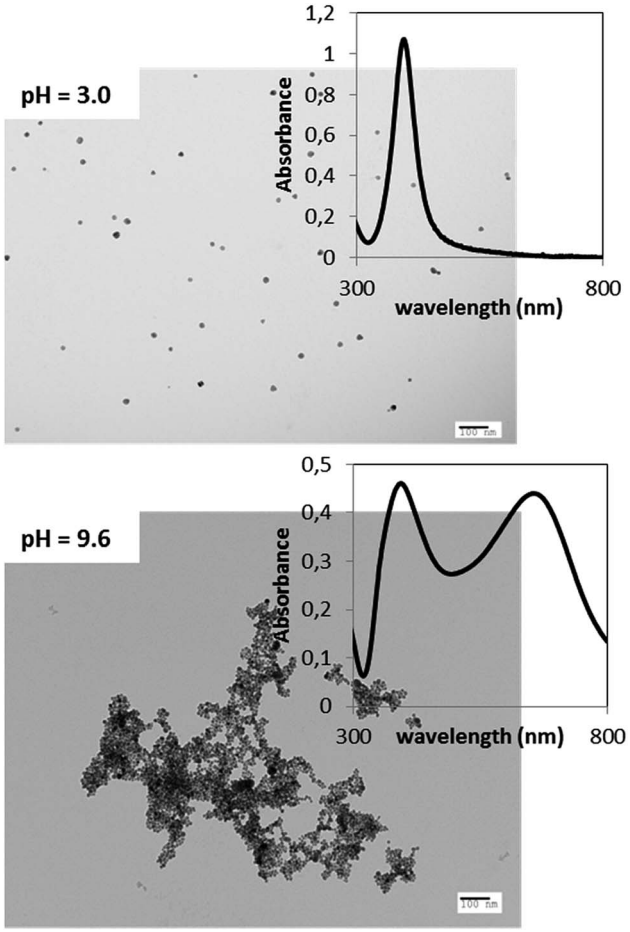

Fig. 5 TEM micrographs of Ag–cysteamine in acidic and basic environments with their corresponding extinction spectra.

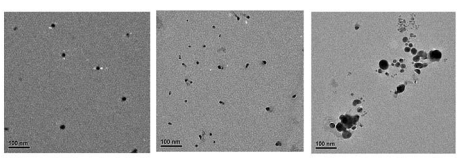

Ionic Strength (mM)	5	10	15
TEM size (nm)	13.5 ± 5	16.8 ± 6	28 ± 15
HDD (nm)	74.5	76.5	65.3

Fig. 6 TEM micrographs and table showing the aggregation of Ag–glycine NPs upon increasing the ionic strength by NaCl.

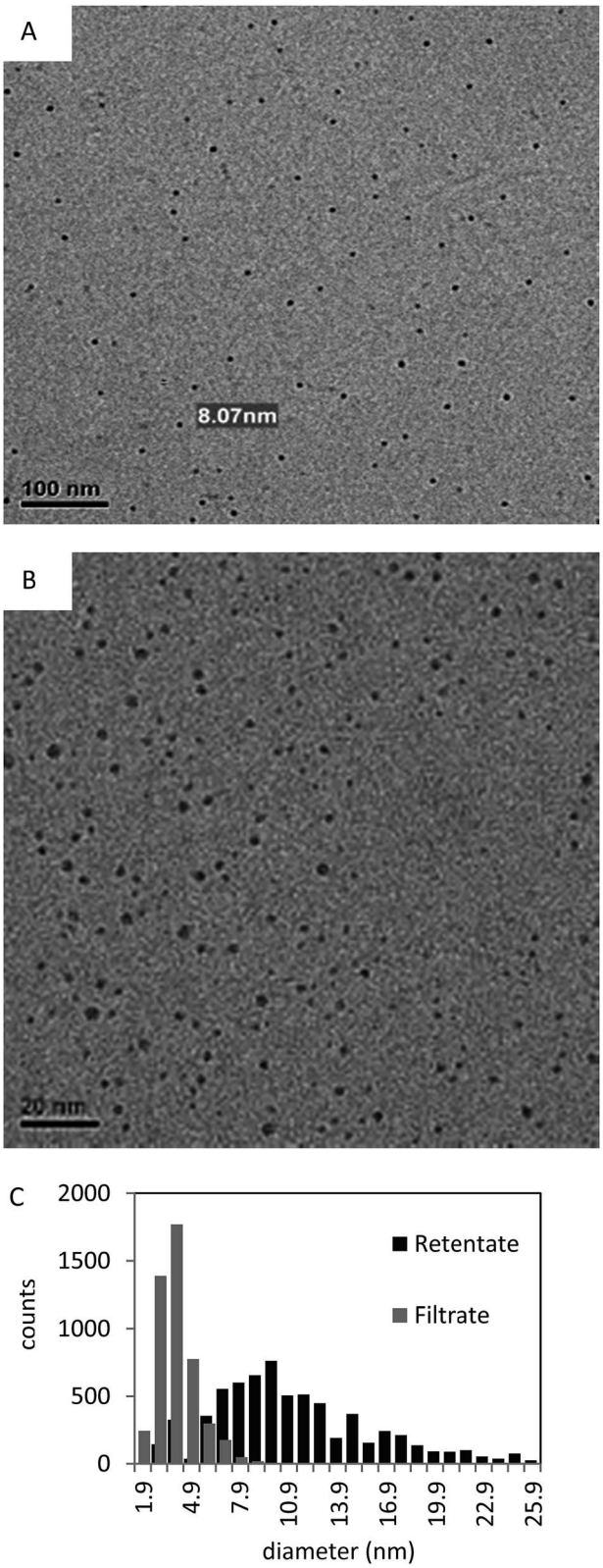

Fig. 7 TEM micrographs showing the Ag–gly sample after filtration through the 100 kDa cellulose membrane: (A) retentate and (B) filtrate. (C) Histogram showing the size distributions of the retentate and filtrate samples.

in ripening and aggregation events when salt is added to the solution.

Although Ag–gly nanoparticles are not stable upon the addition of salt, glycine ligands are quite effective at preventing nanoparticle aggregation in water. Further evidence for the effectiveness of glycine as a stabilizing ligand comes from the ability to reduce sample polydispersity through post-synthesis processing. Potential size purification techniques of nanoparticles include continuous diafiltration[27] and density gradient centrifugation.[28] We observe that the bimodal size distribution of the particles can be successfully resolved by centrifugal filtration through cellulose membranes of MWCO of 100 kDa, which corresponds to an approximately 5 nm pore size. The hydrodynamic diameter as determined by DLS for Ag–glycine NPs is 30 nm. Fig. 7 clearly shows the size separation of the Ag–gly solution and the generation of two Gaussian size populations out of the crude colloid with great NP recovery. The histogram in Fig. 7 shows a reduced recovery of NPs between 4 nm and 8 nm suggesting some degree of irreversible binding to the membrane, while particles outside this range are recovered with low loss. The filtrate size population peaks at 3.9 nm, whereas that of the retentate peaks at 10.0 nm. The choice of the membrane material is crucial to achieve such efficient size purification. Attempts to purify the Ag–gly using PES (polyethersulfone) membranes failed, likely due to irreversible binding of the nanoparticles to the membrane.

Conclusions

In this study, we presented a green and facile stabilization of AgNPs (6–13 nm) by four different short ligands and compared their assemblies, plasmons positions and aggregation behavior. Glycine is believed to bind to the AgNPs surface through the amine group, whereas cysteine, DTT and cysteamine bind preferentially through the sulfhydryl group. Under the appropriate concentration conditions, the cysteine, cysteamine and DTT-stabilized AgNPs show an extended stability in solution. Size purification of Ag–glycine was successful using cellulose membranes of MWCO of 100 kDa. The effect of ligand : Ag ratio on the assembly patterns of cysteine, DTT and cysteamine modified AgNPs is currently under study.

Acknowledgements

The authors wish to thank Dr David Liu for his help with the TEM. They would also like to thank the Canada Foundation for Innovation (CFI), Fonds quebecois de la recherche sur la nature et les technologies (FQRNT), and National Science and Engineering Research Council (NSERC) for providing research support.

References

1 D. Chen, X. Qiao, X. Qiu and J. Chen, Synthesis and electrical properties of uniform silver nanoparticles for electronic applications, *J. Mater. Sci.*, 2009, **44**(4), 1076–1081.
2 S. Paul, C. Pearson, A. Molloy, M. Cousins, M. Green, S. Kolliopoulou, P. Dimitrakis, P. Normand, D. Tsoukalas

and M. Petty, Langmuir–Blodgett film deposition of metallic nanoparticles and their application to electronic memory structures, *Nano Lett.*, 2003, **3**(4), 533–536.

3 (*a*) Z.-J. Jiang, C.-Y. Liu and L.-W. Sun, Catalytic properties of silver nanoparticles supported on silica spheres, *J. Phys. Chem. B*, 2005, **109**(5), 1730–1735; (*b*) R. Xu, D. Wang, J. Zhang and Y. Li, Shape-dependent catalytic activity of silver nanoparticles for the oxidation of styrene, *Chem.–Asian J.*, 2006, **1**(6), 888–893.

4 (*a*) C. J. Murphy, T. K. Sau, A. M. Gole, C. J. Orendorff, J. Gao, L. Gou, S. E. Hunyadi and T. Li, Anisotropic metal nanoparticles: synthesis, assembly, and optical applications, *J. Phys. Chem. B*, 2005, **109**(29), 13857–13870; (*b*) A. D. McFarland and R. P. Van Duyne, Single silver nanoparticles as real-time optical sensors with zeptomole sensitivity, *Nano Lett.*, 2003, **3**(8), 1057–1062.

5 X. Huang, P. K. Jain, I. H. El-Sayed and M. A. El-Sayed, Gold nanoparticles: interesting optical properties and recent applications in cancer diagnostics and therapy, *Nanomedicine*, 2007, **2**, 681–693.

6 P. Alivisatos, The use of nanocrystals in biological detection, *Nat. Biotechnol.*, 2003, **22**(1), 47–52.

7 E. Hao and G. C. Schatz, Electromagnetic fields around silver nanoparticles and dimers, *J. Chem. Phys.*, 2004, **120**(1), 357–366.

8 D. D. Evanoff and G. Chumanov, Size-controlled synthesis of nanoparticles. 1. "Silver-only" aqueous suspensions *via* hydrogen reduction, *J. Phys. Chem. B*, 2004, **108**(37), 13948–13956.

9 N. J. Halas, S. Lal, W.-S. Chang, S. Link and P. Nordlander, Plasmons in strongly coupled metallic nanostructures, *Chem. Rev.*, 2011, **111**(6), 3913–3961.

10 A. M. Gobin, M. H. Lee, N. J. Halas, W. D. James, R. A. Drezek and J. L. West, Near-infrared resonant nanoshells for combined optical imaging and photothermal cancer therapy, *Nano Lett.*, 2007, **7**(7), 1929–1934.

11 C. Sönnichsen, B. M. Reinhard, J. Liphardt and A. P. Alivisatos, A molecular ruler based on plasmon coupling of single gold and silver nanoparticles, *Nat. Biotechnol.*, 2005, **23**(6), 741–745.

12 H. Wang, X. Qiao, J. Chen and S. Ding, Preparation of silver nanoparticles by chemical reduction method, *Colloids Surf., A*, 2005, **256**(2), 111–115.

13 H. Huang and X. Yang, Synthesis of polysaccharide-stabilized gold and silver nanoparticles: a green method, *Carbohydr. Res.*, 2004, **339**(15), 2627–2631.

14 Y. Yin, Z.-Y. Li, Z. Zhong, B. Gates, Y. Xia and S. Venkateswaran, Synthesis and characterization of stable aqueous dispersions of silver nanoparticles through the Tollens process, *J. Mater. Chem.*, 2002, **12**(3), 522–527.

15 H. S. Shin, H. J. Yang, S. B. Kim and M. S. Lee, Mechanism of growth of colloidal silver nanoparticles stabilized by polyvinyl pyrrolidone in γ-irradiated silver nitrate solution, *J. Colloid Interface Sci.*, 2004, **274**(1), 89–94.

16 J. Y. Song and B. S. Kim, Rapid biological synthesis of silver nanoparticles using plant leaf extracts, *Bioprocess Biosyst. Eng.*, 2009, **32**(1), 79–84.

17 A. Troupis, A. Hiskia and E. Papaconstantinou, Synthesis of metal nanoparticles by using polyoxometalates as photocatalysts and stabilizers, *Angew. Chem., Int. Ed.*, 2002, **41**(11), 1911–1914.

18 A. Troupis, T. Triantis, A. Hiskia and E. Papaconstantinou, Rate-Redox-Controlled Size-Selective Synthesis of Silver Nanoparticles Using Polyoxometalates, *Eur. J. Inorg. Chem.*, 2008, **2008**(36), 5579–5586.

19 S. Mandal, A. Gole, N. Lala, R. Gonnade, V. Ganvir and M. Sastry, Studies on the reversible aggregation of cysteine-capped colloidal silver particles interconnected *via* hydrogen bonds, *Langmuir*, 2001, **17**(20), 6262–6268.

20 (*a*) C. A. Mirkin, R. L. Letsinger, R. C. Mucic and J. J. Storhoff, A DNA-based method for rationally assembling nanoparticles into macroscopic materials, *Nature*, 1996, **382**(6592), 607–609; (*b*) A. P. Alivisatos, K. P. Johnsson, X. Peng, T. E. Wilson, C. J. Loweth, M. P. Bruchez and P. G. Schultz, Organization of 'nanocrystal molecules' using DNA, *Nature*, 1996, **382**(6592), 609–611.

21 A. M. E. Badawy, T. P. Luxton, R. G. Silva, K. G. Scheckel, M. T. Suidan and T. M. Tolaymat, Impact of environmental conditions (pH, ionic strength, and electrolyte type) on the surface charge and aggregation of silver nanoparticles suspensions, *Environ. Sci. Technol.*, 2010, **44**(4), 1260–1266.

22 V. V. Apyari, S. G. Dmitrienko, V. V. Arkhipova, A. G. Atnagulov and Y. A. Zolotov, Determination of cysteamine using label-free gold nanoparticles, *Anal. Methods*, 2012, **4**(10), 3193–3199.

23 S. Lin, M. Li, E. Dujardin, C. Girard and S. Mann, One-Dimensional Plasmon Coupling by Facile Self-Assembly of Gold Nanoparticles into Branched Chain Networks, *Adv. Mater.*, 2005, **17**(21), 2553–2559.

24 D.-H. Tsai, M. P. Shelton, F. W. DelRio, S. Elzey, S. Guha, M. R. Zachariah and V. A. Hackley, Quantifying dithiothreitol displacement of functional ligands from gold nanoparticles, *Anal. Bioanal. Chem.*, 2012, **404**(10), 3015–3023.

25 H. Ke, L. Rao, X. Xu and Y. Yan, Density functional theory study of 1: 1 glycine–water complexes in the gas phase and in solution, *Sci. China: Chem.*, 2010, **53**(2), 383–395.

26 S. H. Behrens, D. I. Christl, R. Emmerzael, P. Schurtenberger and M. Borkovec, Charging and aggregation properties of carboxyl latex particles: Experiments *versus* DLVO theory, *Langmuir*, 2000, **16**(6), 2566–2575.

27 S. F. Sweeney, G. H. Woehrle and J. E. Hutchison, Rapid purification and size separation of gold nanoparticles *via* diafiltration, *J. Am. Chem. Soc.*, 2006, **128**(10), 3190–3197.

28 (*a*) G. Chen, Y. Wang, L. H. Tan, M. Yang, L. S. Tan, Y. Chen and H. Chen, High-purity separation of gold nanoparticle dimers and trimers, *J. Am. Chem. Soc.*, 2009, **131**(12), 4218–4219; (*b*) L. Bai, X. Ma, J. Liu, X. Sun, D. Zhao and D. G. Evans, Rapid separation and purification of nanoparticles in organic density gradients, *J. Am. Chem. Soc.*, 2010, **132**(7), 2333–2337; (*c*) F. Bonaccorso, M. Zerbetto, A. C. Ferrari and V. Amendola, Sorting Nanoparticles by Centrifugal Fields in Clean Media, *J. Phys. Chem. C*, 2013, **117**(25), 13217–13229.